Proceedings of ISFOG 2025
5TH INTERNATIONAL SYMPOSIUM ON
FRONTIERS IN OFFSHORE GEOTECHNICS
Nantes, France | June 9-13 2025

ISBN 978-2-85782-758-0

Macro-model of chain-clay interaction for simulating the mooring line pretension in SIMA

S. Rui*
Norwegian Geotechnical Institute, Oslo, Norway

H. P. Jostad, Z. Zhou, Y. Wang
Norwegian Geotechnical Institute, Oslo, Norway

E. Bachynski-Polić, S.Sævik

Department of Marine Engineering, Norwegian University of Science and Technology, Marinteknisk Senter, Trondheim, Norway.

L. Wang, Z. Guo
College of Civil Engineering and Architecture, Zhejiang University, Hangzhou, China

**shengjie.rui@ngi.no (corresponding author)*

ABSTRACT: Traditional fully integrated analyses of floating wind turbines (FWTs) often assume that mooring points are fixed on the seabed, overlooking the complex interactions between the mooring lines and the seabed itself. This simplification fails to account for factors like seabed friction. As a result, it introduces potential inconsistencies and uncertainties into mooring system design, potentially leading to less accurate predictions of performance and safety under varying ocean conditions. This study presents a macro-model integrated into SIMA to simulate the mooring line pretension in clay, capturing the coupled non-linear relationship between displacement and soil reaction forces in three dimensional space. The model was applied to analyze seabed friction and chain embedment effects during the pretension process based on the VolturnUS-S floater with the IEA 15MW floating wind turbine. The study highlights the critical role of modeling the embedded mooring line in accurately capturing seabed friction mobilization. When the embedded portion of the mooring line is not considered, the model predicts higher tension in the mooring lines due to reduced displacement near the padeye on the seabed. This finding underscores the importance of accounting for the embedded line to achieve a more realistic representation of seabed friction between the mooring line and the seabed.

Keywords: Anchor chain; Mooring line; Floating wind turbine; Macro-model; Pretension

1 INTRODUCTION

Offshore floating wind turbines (FWTs) are promising for reducing CO_2 emissions, especially in waters deeper than 60 m. Mooring systems, including mooring lines and anchors, are vital for their stability under various conditions (Zhou et al., 2021; Zhang et al., 2023). Compared to mooring systems for oil and gas platforms, mooring systems for FWTs not only resist wave-induced loads but also significant wind forces, which presents unique design challenges (Xu et al., 2023a; Rui et al., 2024a). Cost sensitivity in FWTs further complicates the design process, as overly conservative designs can hinder commercial viability. As FWT farms expand, optimizing mooring line and anchor designs will be crucial to balancing safety with cost-efficiency.

Mooring lines for floating wind turbines typically consist of two segments: the suspended line in the water and the embedded line in the seabed, especially when using suction or drag anchors (Shen et al., 2019). Numerous studies have investigated the configuration and tension distribution of suspended lines (Leonard & Nath, 1981; Vallabhan, 2008; Xu et al., 2021), often utilizing commercial software like SIMA, OrcaFlex, and ANSYS AQWA. Despite extensive research, many studies tend to oversimplify the interaction between mooring lines and seabed, often assuming a fixed attachment point at the mudline and neglecting the effects of the embedded mooring segment **(Figure 1(a)**). In practice, the load attachment points (padeyes) of anchors such as suction and drag anchors are deeply embedded below the mudline, creating a reverse catenary shape for the embedded portion of the mooring line during operation (Rui et al., 2021a; Xu et al., 2023b), which influences system behavior **(Figure 1(b)**). Moreover, common modeling approaches, such as linear springs

or elastic foundation methods, are often used to represent the mooring line lying on the seabed. However, these methods fail to capture the intricate interactions between the mooring line and seabed, leading to less accurate simulations of the system's behavior.

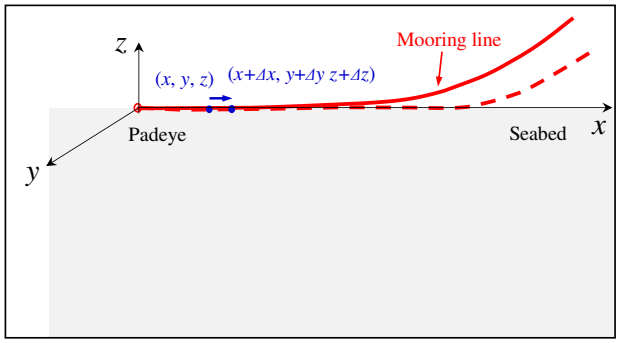

(a) traditional model in commercial software

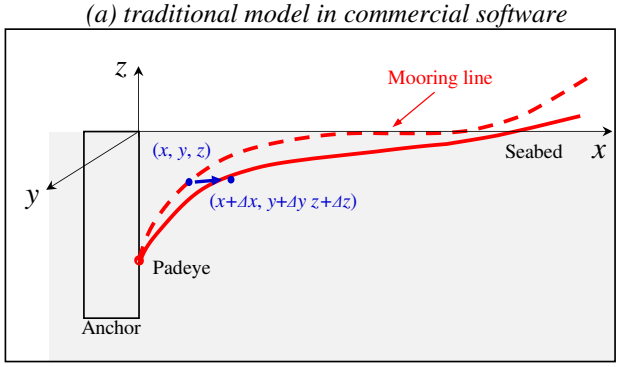

(b) actual mooring line state

Figure 1. Mooring line-seabed interaction

Wung et al. (1995) utilized a linear spring and dashpot model to simulate the dynamic contact between mooring chain and clay seabed. Xiong et al. (2016, 2017) applied the lumped mass method to analyze dynamic tensions and load directions at the fairlead and anchor pad-eye. Shen et al. (2019) conducted numerical studies on the dynamic behavior of mooring chains in clay and sand, highlighting that cyclic movements of the floater can cause tension relaxation in the mooring line. Rui et al. (2021b) studied load transfer from the fairlead to the pad-eye using a dynamic mooring line model, finding that inertia and soil reaction forces affect tension variations. Wang et al. (2020) and Rui et al. (2023) developed numerical methods to predict two-dimensional (2D) and three-dimensional (3D) trench profiles, emphasizing the role of embedded line-soil interactions in mooring line dynamics.

Integrated analysis is crucial in floating wind turbine design to minimize uncertainties and reduce costs. While current numerical models effectively capture aero-hydro-servo-elastic interactions, commercial software like SIMA often oversimplifies mooring line-seabed interactions by assuming a fixed seabed point. Incorporating a detailed mooring line-seabed interaction model is essential for more accurate FWT response assessments and reducing failure risks.

This study presents a macro-model integrated in SIMA to simulate the interaction between mooring lines and seabed soil, capturing the coupled non-linear relationship between displacement and soil reaction forces in 3D. The model was applied to analyze seabed friction and chain embedment effects during the pretension process based on the VolturnUS-S floater with the IEA 15MW floating wind turbine.

2 MACRO-MODEL OF CHAIN-SEABED INTERACTION

2.1 Basic assumptions

Macro-models provide an efficient approach for simulating interactions between structures and surrounding soil, using a framework similar to soil constitutive models, like the elasto-plastic approach (Aubeny et al., 2003; Houlsby, 2016; Page et al., 2018). This study introduces macro-models to simulate the mooring line pretension in SIMA. Unlike traditional methods in SIMA that assume a fixed point at the mudline, these macro-models account for the embedded mooring chain, offering more accurate analyses of mooring systems.

The macro-model is based on the following assumptions:

1. Flat seabed: The seabed is considered flat, without the effects of trenches or scour.
2. Undrained seabed clay: The seabed clay remains in undrained conditions throughout the simulation.
3. Embedded anchor padeye: The anchor padeye is assumed to remain fixed at a specific depth.

2.2 Macro-model description

Figure 2 shows macro-element for mooring line-soil interaction. To model soil reaction forces on the embedded mooring chain, two macro-elements are introduced at each node along the mooring line, with each representing the half of a mooring line segment in front of or behind the node.

The variations in local soil reaction forces (ΔS_t, ΔS_{n1}, ΔS_{n2}) in tangential, normal and binormal directions are calculated using elastic stiffnesses.

$$\Delta S_t = K_t \Delta v_t \quad (1a)$$

$$\Delta S_{n1} = K_n \Delta v_{n1} \quad (1b)$$

$$\Delta S_{n2} = K_n \Delta v_{n2} \quad (1c)$$

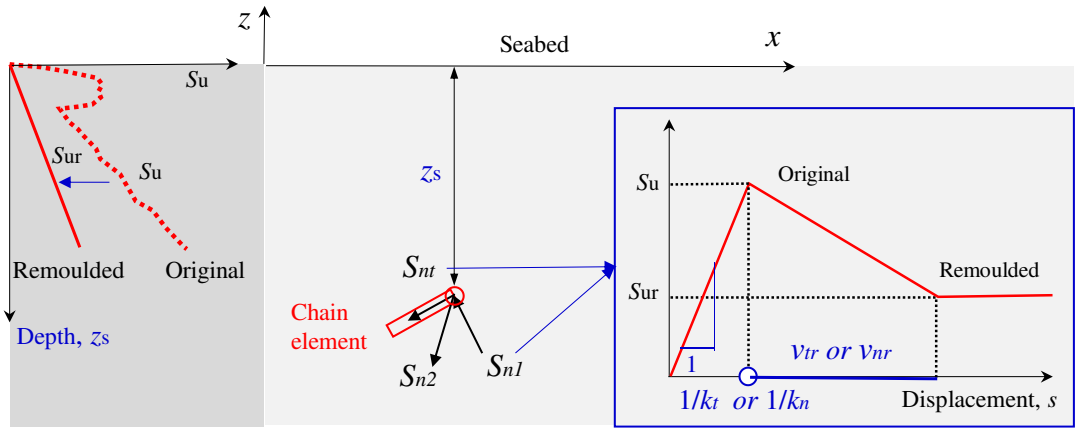

Figure 2. Macro-element for mooring line (chain) – soil interaction

where Δv_t, Δv_{n1} and Δv_{n2} represent the displacements in the tangential, normal, and binormal directions, respectively; the elastic stiffness components are formulated by:

$$K_t = k_t T_f \quad (2a)$$

$$K_n = k_n N_f \quad (2b)$$

where k_t and k_n are the stiffness values, related to the mooring line diameter, d_e. Note that the same normal stiffness K_n is adopted in the two normal directions (n_1, n_2). T_f and N_f are the tangential and normal yield forces, calculated by:

$$T_f = E_t d_b s_u \Delta L/2 \quad (3a)$$

$$N_f = E_n d_b N_c s_u \Delta L/2 \quad (3b)$$

where d_b is the nominal chain diameter; E_t and E_n are effective width parameters in the normal and tangential directions, respectively; N_c is the bearing capacity factor; s_u represents the isotropic undrained shear strength; ΔL is the segment length. In this study, $s_u = s_{ur} = 1.5 z_s$ kPa (where s_{ur} is the residual undrained shear strength, z_s is the segment depth) is adopted. It indicates that the plastic displacement to reach residual undrained shear strength v_{tr} and v_{nr} is infinite.

2.3 Parameter determination

Due to the irregular geometry of mooring chain, directly determining the soil reaction force is challenging. For clay, Degenkamp & Dutta (1989) recommended that E_t=8 and E_n=2.5 for a fully embedded chain seabed, which is adopted in this study. Liu et al. (2024) analyzed other values of E_t, which are slightly larger than the value adopted in this study.

Table 1 presents key input parameters for the macro-models to calculate soil reaction forces. For a chain with a nominal diameter d_b of 0.185 m (as adopted in the subsequent simulation for the floating wind turbine), k_n=10.8 and k_t=5.4 are adopted. The normal and tangential displacements (s_n and s_t) required to achieve E_n=2.5 and E_t=8 are calculated as $s_n = 0.5 E_n d_b$ and $s_t = E_n d_b$, respectively.

Table 1 Key inputs in the macro-model

Parameters	Expressions	Values (d_b=0.185 m)
k_n	$2/d_b$	10.8 m^{-1}
k_t	$1/d_b$	5.4 m^{-1}
s_n	$0.5E_n d_b$	0.23 m
s_t	$E_n d_b$	0.46 m

3 SIMULATION CASES

3.1 Wind turbine and mooring system

This study simulates the mooring line pretension of the mooring system for the VolturnUS-S floater supporting the IEA 15MW floating wind turbine. Key mooring system parameters are detailed in **Table 2**.

The mooring system for the IEA 15MW FWT in 200 m water depth includes three mooring lines, spaced 120° apart. The anchor padeye is at a depth of 210 m, with the fairlead positioned 14 m below sea level. Anchors are 837.6 m from the platform centerline, and each mooring line is 850 m long with a diameter of 0.185 m. As shown in **Figure 3(a),** in a catenary system with the padeye on the seabed, seabed friction is not considered. Under the condition, the fairlead pretension (2437 kN) following the traditional method in **Figure 3(a)** is caused by the chain self-weight.

Table 2 Key parameters of the mooring system for IEA 15MW floating wind turbine

Parameters	Values
Number of mooring lines	3

Angle between adjacent mooring lines	120°
Depth of anchor padeye below sea level	210 m
Fairlead radial spacing	58 m
Depth to fairlead below sea level	14 m
Radius to anchors from platform centerline	837.60 m
Unstretched mooring line length	850 m
Line Breaking Strength	22286 kN
Mooring line diameter	0.185 m
Equivalent mooring line mass density	685 kg/m
Fairlead pretension	2437 kN
Fairlead angle from SWL	56.4°
Axial stiffness	3270 MN

3.2 Pretension process

Before determining the static configuration of a mooring line, a pretension process is required. For example, with a suction anchor, a vertical mooring line is attached to the anchor embedded in the seabed and connected to a chain lying on the seabed. During pretensioning, the chain is lifted and connected to a third segment, which is then towed to the fairlead on the floating platform. The initial pretension is set by adjusting the mooring line length.

In conventional methods using SIMA, where a fixed seabed point is assumed, the initial mooring line configuration process is shown in **Figure 3(a)**. The mooring line starts as a horizontal line suspended in water, with endpoints simultaneously connected to the padeye at the mudline and the fairlead on the floater. This approach does not fully account for seabed friction, potentially overestimating the load on the anchor.

This study introduces a novel method to determine the initial configuration by accounting for seabed friction and the embedded chain, as illustrated in **Figure 3(b)**. After installing a suction anchor, a vertical mooring line L_1 in the seabed is connected to the lying chain L_2. When all components are in place, the upper end of the mooring line is lifted, forming segment L_3. The red and black lines depict the mooring line configuration before and after the pretension process in SIMA.

During the pretension process, the upper end is pulled to connect with the floating structure, embedding segment L_1 fully into the seabed and partially embedding segment L_2, with the rest lying on the seabed.

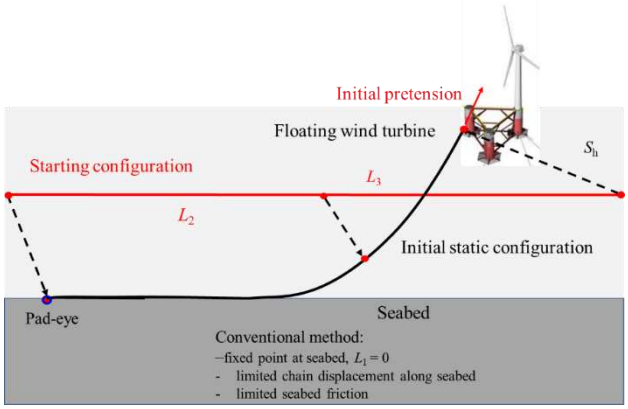

(a) traditional method

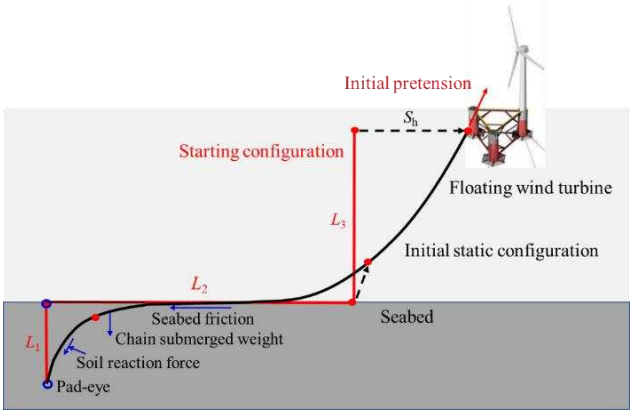

(b) method in this study

Figure 3 – Pretension process simulation of mooring line in SIMA

4 RESULT

Traditional methods often exclude the embedded line, necessitating a comparison of different approaches. In the first case, the mooring line is 850 m long with a padeye embedded 10 m deep. The second case has an 840 m line, excluding the embedded segment L_1, with the padeye on the mudline. The third case uses an 850 m line with the padeye on the mudline, highlighting the impact of the embedded segment with the same total length. All other parameters remain constant across cases, allowing for a clear assessment of the

embedded segment's influence on mooring performance.

4.1 Mooring line configuration

Figure 4 compares mooring line configurations with and without the embedded line. The presence of the embedded segment (L_1) in Case 1 significantly affects the overall configuration and shifts the touchdown point closer to the anchor compared to Case 2, where L_1 is absent. While Case 2 has a shorter mooring line length (840 m) compared to Case 1 (850 m), both Case 1 and Case 3 have a total length of 850 m, with the configuration in Case 1 positioned above that of Case 3 due to the embedded segment.

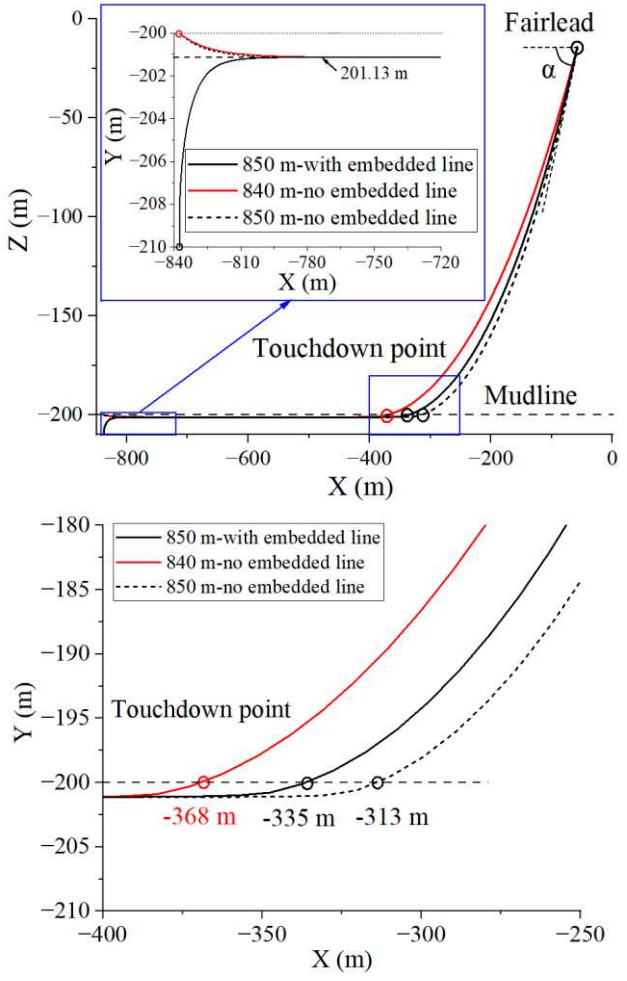

Figure 4. Comparison between mooring line configurations with and without the embedded line

4.2 Mooring line tension

Figure 5 compares mooring line tensions with and without the embedded segment L_1. Without L_1 (Case 2), the mooring line experiences higher tension (with 3059 kN at the fairlead),14.6% greater than with the embedded line (Case 1). From the touchdown point, the axial reaction force decreases linearly in both cases. For Cases 1 and 3, both with a total length of 850 m, the tension without the embedded line is 2462 kN, a 7.6% reduction compared to Case 1, but with a higher tension at the padeye (960 kN) due to limited seabed friction. In Cases 2 and 3, tension decreases more slowly without the embedded line, as minimal displacement near the padeye limits friction mobilization, whereas the embedded line allows sufficient displacement to fully engage seabed friction.

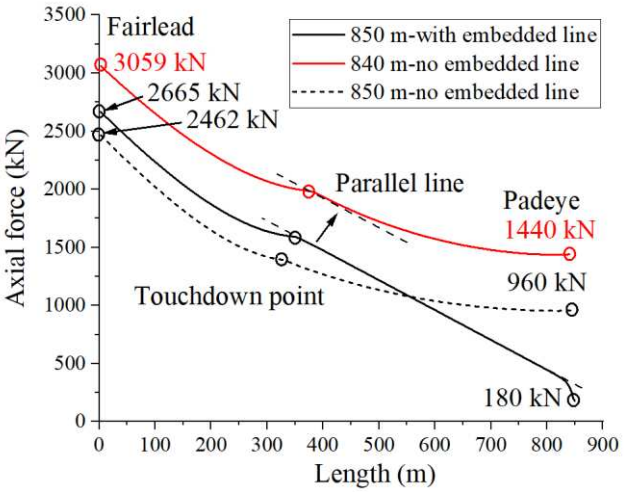

Figure 5. Comparison between the mooring line tensions with and without the embedded line

5 CONCLUSIONS

This study presents a macro-model integrated into SIMA to simulate the interaction between mooring lines and seabed soil, capturing the coupled non-linear relationship between displacement and soil reaction forces in 3D. It evaluates seabed friction and chain embedment effects during the pretension process. The model was applied to static mooring analyses of the VolturnUS-S floater with the IEA 15MW floating wind turbine. Main conclusions are as follows:

(1) The proposed macro-model can simulate the behaviour of embedded lines. The results reveal that mooring lines without an embedded section experience higher tension at the padeye. This is because, with the padeye on the seabed, the displacement near it is too small to fully mobilize seabed friction.

(2) The embedded mooring line not only resists a portion of the tension transferred from the touchdown point but also allows sufficient displacement of the lying chain to mobilize seabed friction.

(3) Accurately accounting for seabed friction requires careful consideration during the pretension stage, and this proposed model can simulate the mobilization of seabed friction.

AUTHOR CONTRIBUTION STATEMENT

First Author: Software, Data curation, Formal Analysis, Writing- Original draft. **Second, Third and Fourth Author**: Conceptualization, Methodology. **Fifth and Sixth Authors**: Visualization, Supervision. **Seventh and Last Author**: Supervision, Writing- Reviewing and Editing.

ACKNOWLEDGEMENTS

The authors are grateful for the financial support provided by the European Commission (HORIZON-MSCA-2022-PF-01, 101108745) and the Research Council of Norway (SFI BLUES project, 309281).

REFERENCES

Aubeny, C. P., Han, S. W., & Murff, J. D. (2003). Inclined load capacity of suction caissons. *International Journal for Numerical and Analytical Methods in Geomechanics*, *27*(14), 1235-1254.

Degenkamp, G., & Dutta, A. (1989). Soil resistances to embedded anchor chain in soft clay. Journal of Geotechnical Engineering, 115(10), 1420-1438.

Houlsby, G. T. (2016). Interactions in offshore foundation design. *Geotechnique*, *66*(10), 791-825.

Leonard, J. W., & Nath, J. H. (1981). Comparison of finite element and lumped parameter methods for oceanic cables. *Engineering structures*, *3*(3), 153-167.

Liu, W., Tian, Y., Cassidy, M. J., O'Loughlin, C., & Watson, P. (2024). Numerical Investigation of the Capacity of Anchor Chain Links in Clay. *Journal of Geotechnical and Geoenvironmental Engineering*, *150*(10), 04024090.

Page, A. M., Grimstad, G., Eiksund, G. R., & Jostad, H. P. (2018). A macro-element pile foundation model for integrated analyses of monopile-based offshore wind turbines. *Ocean Engineering*, *167*, 23-35.

Rui, S., Guo, Z., Wang, L., Liu, H., & Zhou, W. (2021a). Numerical investigations on load transfer of mooring line considering chain–seabed dynamic interaction. *Marine Georesources & Geotechnology*, *39*(12), 1433-1448.

Rui, S., Zhou, Z., Gao, Z., Jostad, H. P., Wang, L., Xu, H., & Guo, Z. (2024a). A review on mooring lines and anchors of floating marine structures. *Renewable and Sustainable Energy Reviews*, 199, 114547.

Rui, S., Zhou, Z., Jostad, H. P., Wang, L., & Guo, Z. (2023). Numerical prediction of potential 3-dimensional seabed trench profiles considering complex motions of mooring line. *Applied Ocean Research*, *139*, 103704.

Shen, K., Guo, Z., & Wang, L. (2019). Prediction of the whole mooring chain reaction to cyclic motion of a fairlead. *Bulletin of Engineering Geology and the Environment*, 78, 2197-2213.

Vallabhan, C. G. (2008). Two-dimensional nonlinear analysis of long cables. *Journal of engineering mechanics*, *134*(8), 694-697.

Wang, L., Rui, S., Guo, Z., Gao, Y., Zhou, W., & Liu, Z. (2020). Seabed trenching near the mooring anchor: History cases and numerical studies. *Ocean Engineering*, *218*, 108233.

Wung, C. C., Litton, R. W., Mitwally, H. M., Bang, S., & Taylor, R. J. (1995, May). Effect of soil on mooring system dynamics. In *Offshore Technology Conference* (pp. OTC-7672). OTC.

Xiong, L., White, D. J., Neubecker, S. R., Zhao, W., & Yang, J. (2017). Anchor loads in taut moorings: The impact of inverse catenary shakedown. *Applied Ocean Research*, *67*, 225-235.

Xiong, L., Yang, J., & Zhao, W. (2016). Dynamics of a taut mooring line accounting for the embedded anchor chains. *Ocean Engineering*, *121*, 403-413.

Xu, H., Rui, S., Shen, K., & Guo, Z. (2023b). Investigations on the mooring safety considering the coupling effect of the mooring line snap tension and anchor out-of-plane loading. *Applied Ocean Research*, *141*, 103753.

Xu, H., Rui, S., Shen, K., Jiang, L., Zhang, H., & Teng, L. (2023a). Shared mooring systems for offshore floating wind farms: A review. *Energy Reviews*, 100063.

Xu, K., Larsen, K., Shao, Y., Zhang, M., Gao, Z., & Moan, T. (2021). Design and comparative analysis of alternative mooring systems for floating wind turbines in shallow water with emphasis on ultimate limit state design. *Ocean Engineering*, *219*, 108377.

Zhang, H., Guo, Z., Wang, L., Rui, S., Zhu, R., & Zhang, X. (2023). Numerical investigations on the installation of dynamically installed anchors with attached mooring line. *Applied Ocean Research*, *139*, 103716.

Zhou, W., Guo, Z., Wang, L., Zhang, Y., & Rui, S. (2021). Numerical model for suction caisson under axial cyclic loadings. *Ocean Engineering*, *240*, 109956.